Simulations of tidal turbine blade loading in flood and ebb tides

Christopher R. Vogel, Tianning Tang, Sergio L. Dubon and Jeff Steynor

Abstract—**Tidal turbines are deployed for extended periods in a harsh environment with significant levels of flow-induced unsteady loading. The contributions of these loads to fatigue damage of the turbine blades is not well understood, contributing to over-engineered structures with attendant cost penalties in order to avoid premature failure. In this paper, we investigate computationally the effect of the velocity shear profile during the flood and ebb tides on the unsteady loading of a tidal turbine. The flow profiles are based on data from the Fall of Warness, UK. Actuator line simulations of a fixed-speed turbine were performed to evaluate the spanwise blade loading distribution and blade root shear forces and bending moments. The magnitude of load fluctuations were observed to increase with flow speed due to the larger onset flow variation across the rotor plane. This effect was amplified during the flood tide due to the greater shear across the rotor plane, reaching almost 20% at a hub-height flow speed of $3.0\,\mathrm{ms}^{-1}$, whereas a surface stress during the ebb tide acted to suppress the variation in flow speed across the rotor plane. This was also reflected in the blade root shear force and bending moments, with greater azimuthal variation experienced during flood tides than in the ebb tide. The spanwise load distributions generated in this work are being used to define the loads that will be applied to a decommissioned tidal turbine blade in the accelerated cyclic blade testing facility FastBlade.**

Index Terms—**Actuator line simulations, Reynolds-Averaged Navier-Stokes Simulation, Tidal Stream Turbines**

I. Introduction

TIDAL stream turbines operate in a harsh marine environment, characterised by significant levels of flow unsteadiness. This unsteadiness can give rise to blade load fluctuations which results in fatigue damage of the turbine. This is of particular concern given the 10-20 year operating life expected from the turbines, and the considerable uncertainty about blade loads has been attributed as a cause of some early tidal turbine failures [1].

Flow unsteadiness arises from deterministic and stochastic sources [2]. Deterministic sources of unsteadiness include the vertical shear profile, tower passing and tidal fluctuations [3]. Blades experience a once-per-revolution (1p) load fluctuation as they rotate through the shear profile, causing a 3p variation in rotor thrust and torque. Stochastic sources of flow unsteadiness include surface waves, free-stream turbulence and, for turbines mounted on floating platforms, platform-induced motions. All sources of flow unsteadiness can have a significant impact on the loads experienced by the turbine blades, in particular the fatigue loading that they generate. Therefore, it is important to consider the impact of unsteady loads as part of the blade design process in order to avoid premature failure.

Despite the outward similarities between wind and tidal horizontal-axis turbines, there are a number of key differences between their operating environments when evaluating unsteady blade loads. Tidal turbine blades tend to be much shorter and the number of plies in composite materials changes more rapidly radially than their wind turbine counterparts. The vertical shear profile is particularly significant at shallower tidal sites [4], such as the approximately 30-60 m water depth at many sites considered suitable for turbine deployment [5]–[8]. Consequently, tidal turbines in general experience a much greater variation in onset flow that most large wind turbines, although small wind turbines, which operate lower in the atmospheric boundary layer, can also experience significant flow speed variations across the rotor plane [9].

The size and positioning of the turbine has an important role in determining how large the flow speed variations due to the shear profile are; an average difference between the velocity at the lowest blade position and the average (power-weighted) flow speed over the rotor of $0.07\,\mathrm{ms}^{-1}$ was reported for the 4 m diameter Schottel turbine, which is supported from a floating platform [10]. Lab-scale turbines tend to occupy a more substantial portion of the water column, and hence a greater impact due to velocity shear has been observed. For example, recent experiments conducted at IFREMER, where the turbine diameter of 0.9 m occupies 45% of the water depth (2 m), found that the magnitude of root bending moment variations increased closer to the free surface. However, the mean loads were lower due to interactions with surface waves [11]. Turbines may be deployed in closely-spaced arrangements to minimise support infrastructure and to exploit constructive interference effects. Blade passage near adjacent turbines or the seabed and surface has been observed to also contribute to periodic load fluctuations [12], [13].

Wind turbines, especially large ones, can also experience significant gravity-driven load cycles, whereas

This work was supported by the Supergen Offshore Renewable Energy Hub under grant FF2020-1063.

C. R. Vogel is at the Department of Engineering Science, University of Oxford, Oxford OX1 3PJ, United Kingdom (email: christopher.vogel@eng.ox.ac.uk)

T. Tang is at the Department of Engineering Science, University of Oxford, Oxford OX1 3PJ, United Kingdom (email: tianning.tang@eng.ox.ac.uk)

Sergio Dubon is at the School of Engineering, University of Edinburgh, Edinburgh EH9 3FB, United Kingdom (email: sergio.ldubon@ed.ac.uk)

J. Steynor is at the School of Engineering, University of Edinburgh, Edinburgh EH9 3FB, United Kingdom (email: jeff.steynor@ed.ac.uk)

this effect is largely mitigated by blade buoyancy in tidal applications. However, ambient levels of turbulence tend to be higher in tidal flows compared to offshore winds, which also contributes significantly to the load fluctuations experienced by the turbines. The largest tidal eddies can have length scales in excess of the water depth, which is not observed in wind.

The impact of unsteady loads on full size tidal turbines is challenge to analyse due to the variation in the mean velocity and velocity shear profile throughout the tidal cycle [14]. Differences have been observed in turbine power curves between flood and ebb tide due to differences in shear profile and turbulence intensity [15]. Tidal velocities vary in a periodic and thus predictable manner, whereas Weibull or Rayleigh probability distributions are used to describe the variability of mean wind speed. Simulations of a full size tidal turbine at the Fall of Warness site performed by Ahmed et al. demonstrated individual blade load variations of approximately $\pm 10\%$ due to the cyclical effects of velocity shear and tower passing in low onset turbulence flows [16]. It was found that blade-generated turbulence had only a minor effect on blade load fluctuations, but that high levels of onset turbulence, achieved using synthetic eddies, can significantly increase the magnitude of fluctuations.

Differences in the velocity shear profile throughout a tidal cycle can be exacerbated by the contribution of surface waves, in particular if the wave direction opposes the tidal current. This leads to steeper waves and greater blade load fluctuations [17]. The velocity shear profile also varies significantly from site to site; despite both sites having similar water depths, flow speeds above 10 m from the seabed at the Fall of Warness [6] vary much more with height than that in the Petit Passage, Bay of Fundy [18].

The severe consequences of fatigue loads on turbine lifetime has led to work on active and passive control methods to alleviate some of the fatigue damage experienced by turbines. Active control methods include the use of active flaps and blade pitch and/or speed control of the turbine [19]. Passive methods utilise the deflection of the blade in operational conditions to relieve some of the blade loads, and have the advantage of not requiring additional mechanical systems [20]. However, it is still important to understand loads fluctuations experienced by turbines in any lifetime performance assessment.

This work is part of the Supergen ORE hub-funded LoadTide project (FF2020-1063) which seeks to evaluate lifetime fatigue loads on a full-size tidal turbine blade. Recreating the loading on the blade requires that the variation in spanwise force distribution is determined considering the different flow speeds and shear profiles encountered throughout the ebb-flood tidal cycle. The simulated flow conditions are based on observations from the Fall of Warness European Marine Energy Centre (EMEC) site in Orkney. In this work, we employ unsteady simulation with actuator line turbine representation in order to capture the once-per-revolution sampling of the oncoming flow profile by the blades.

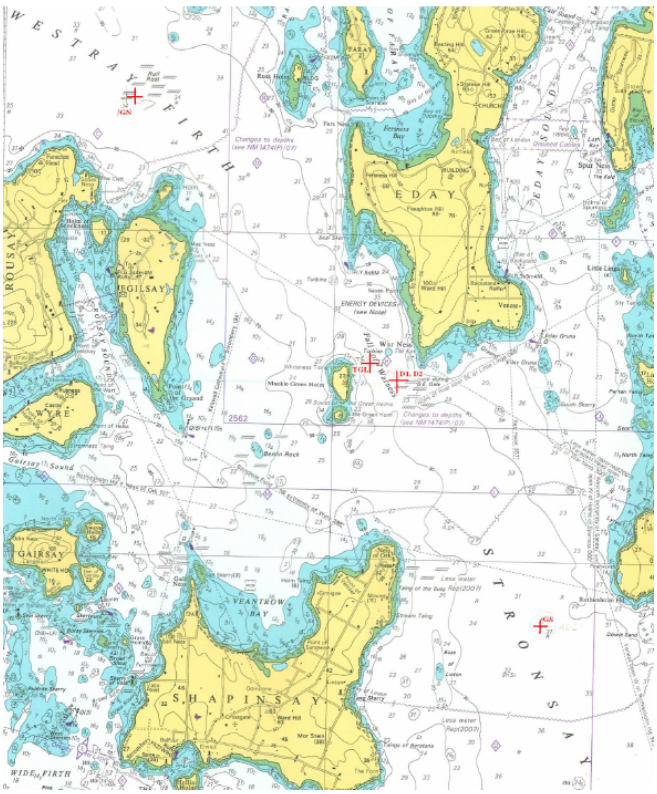

Fig. 1. Map of the Westray Firth and Stronsay Firth, marking the Fall of Warness site, location of the ReDAPT project, at the centre of the map. Sourced from Sellar & Sutherland [6] based on an Admiralty chart.

II. Flow profiles

The flow data used in this data were sourced from the ReDAPT project at the Fall of Warness, EMEC, Orkney UK [6], [21], [22]. A map of the site is shown in Fig. 1. The data were collected using two acoustic Doppler current profilers that were deployed between 19 July and 2 August 2013. The profilers were positioned 0.8 m above the seabed, and sampled the flow at a frequency of 0.5 Hz. The mean operating depth of the profilers during deployment was 43.2m and 46.2m due to the slightly different seabed conditions at their respective locations.

Flow speed and turbulence intensity data were binned into mean hub-height flow speed bins of $U_\infty = (0.7,\ 1.4,\ 2.1,\ 2.8,\ 3.0,\ 3.5)$ ms^{-1} for both the flood and ebb tides, noting that $U_\infty = 3.5$ms^{-1} was only achieved during the ebb tide. Data were only included if the wave height was less than 1 metre. The ensemble length for all statistics was 5 minutes, and a 0.12cm s^{-1} noise correction estimate was made to the turbulence intensity data following [6].

Vertical profiles of flow speed and turbulence intensity are presented in Fig. 2, demonstrating the differences in the profiles between the ebb and flood tides. A surface stress due to the wind is particularly noticeable during the ebb tides, which means that the fastest flows were encountered about half way through the water column at the highest flow speed bins. This also gives rise to the differences in the turbulence intensity profiles between the flood and ebb tides. Consequently, the standard deviation of the flow speed across the

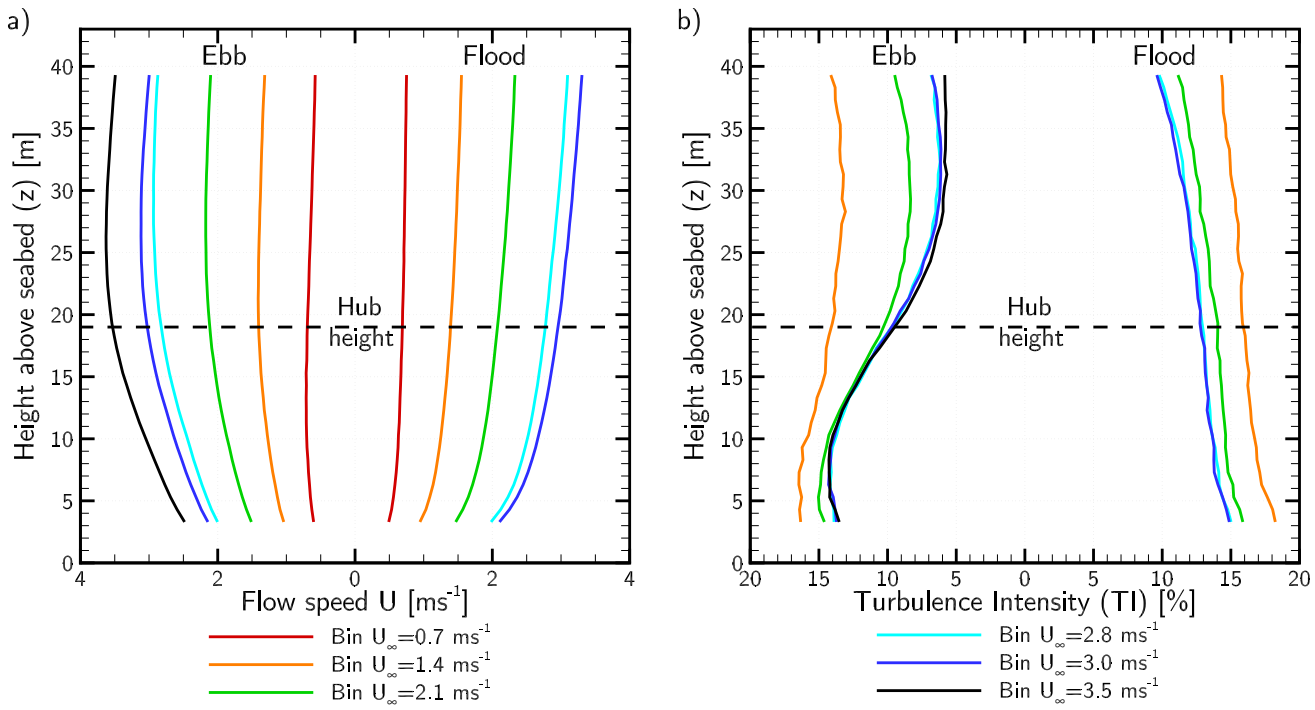

Fig. 2. Simulated vertical profiles of (a) flow speed (u) and (b) turbulence intensity (TI) at the Fall of Warness ReDAPT site, based on [6]. Data binned by mean hub-height velocity for ebb and flood tide conditions. The turbine hub-height, 19 m above the seabed, is indicated with a horizontal dashed line.

rotor plane is consistently higher for flood tides than the ebb tides, for a specified hub-height flow speed, as shown in Table I.

During the flood tide, the velocity profiles follow an approximately $1/6^{\text{th}}$ power law, whereas this is closer to a $1/5^{\text{th}}$ power law for the ebb tide for the lower portion of the flow unaffected by the surface shear stress.

TABLE I
STANDARD DEVIATION IN SIMULATED FLOW SPEED ACROSS THE ROTOR PLANE IN FLOOD AND EBB TIDES AS A FUNCTION OF HUB-HEIGHT FLOW SPEED.

Hub-height flow speed bin [ms^{-1}]	Ebb tide	Flood tide
0.7	0.0429	0.0639
1.4	0.0944	0.1546
2.1	0.1889	0.2257
2.8	0.2782	0.2866
3.0	0.2833	0.3123
3.5	0.3331	-

III. TURBINE PROPERTIES

The turbine used in this investigation is based on a full-scale tidal turbine; some details are omitted due to commercial sensitivity. The rotor radius $R = 9$ m and nacelle radius $R_{hub} = 1.35$m. Consequently, the span of the blade is $0.137 \leq r/R \leq 1.0$. The turbine hub-height was taken to be 19 m above the seabed, such that the turbine is approximately centred in the water column. The blade twist $\beta(r)$ and chord $c(r)$ reduce smoothly with radius outboard of $r/R = 0.228$, within the range $23.2° \leq \beta \leq 2.8°$ and 2.271 m $\leq c(r) \leq 0.600$ m. The blade is blended into a cylindrical cross-section between $0.139 \leq r/R \leq 0.228$ with $c = 1.612$ m to aid connection into the nacelle.

The blade cross-section is defined by the NACA 63-4XX aerofoil series, where XX represents represents the thickness-to-chord ratio along the blade. The blade thickness-to-chord ratio decreased moving outboard along the blade from 55% at $r/R = 0.228$ to a minimum of 18% at the blade tip. The innermost portion of the blade, between $0.139 \leq r/R \leq 0.228$ was taken to have a cylindrical cross-section, with an implied thickness-to-chord ratio of 100%.

NACA aerofoil coordinates were determined following NASA reference [23], with the geometry sampled at 300 equally-spaced points. Aerofoil lift and drag characteristics as a function of angle of attack α were computed using QBlade [24] with the chord-based Reynolds number $Re = \rho V(r)c(r)/\mu$ in the range between $10\times10^6 <$ Re $< 18\times10^6$, where ρ and μ are the density and dynamic viscosity of air respectively, and $V(r)$ is the flow speed relative to the blade at radius r. The critical number $N_{crit} = 9$ for all cases. A fixed rotor speed of 13.78 rpm was assumed.

IV. COMPUTATIONAL MODEL

A suite of unsteady Reynolds-Averaged Navier Stokes (URANS) simulations were performed using the computational fluid dynamics (CFD) solver OpenFOAM (version 2.3.1). The choice of URANS simulation draws on the work of Ahmed et al. which found that URANS and Large Eddy Simulation predict very similar phase-averaged loads and blade pressure distributions in low onset turbulence flows [16], as is the

focus of this paper. The simulations were performed using the PimpleFoam PISO algorithm and turbulence closure was provided by the $k-\omega$ SST model with the 2003 updated coefficients [25]. The simulated time for each case was 400s, with a time step of 0.03s.

A. Computational domain

The computational domain was 250 m long, 520 m wide and 43 m tall, corresponding to the height of the ReDAPT site. The width of the domain was set to achieve a small geometric blockage ratio (ratio of rotor swept area to channel cross-sectional area) of 1.14%. A vertical flow profile was imposed at the inlet of the computational domain using atmospheric boundary layer inlet condition. The flow profile was sustained by a no-slip wall boundary condition at the bottom of the domain and a stress boundary condition at the top. At the outlet boundary, the static pressure was set to a fixed value of 0 Pa, and zero gradient boundary conditions were applied to the turbulence and velocity scalars. Symmetry conditions were applied to the lateral boundaries of the domain. The inflow and top boundary conditions were adjusted to achieve a close match to the flow profile observed from the ReDAPT data.

B. Meshing strategy

The domain was discretised with an Octree mesh to allow a concentration of resolution near the rotor region. Convergence of the mesh parameters was evaluated through comparison of the simulated flow profile to the field observations described in Section II and the spanwise distribution of blade forces.

A spatially-homogeneous grid dimension of 1.5 m was found to capture well the velocity gradients near the seabed and surface boundaries and provide good agreement with field observations of the mean velocity profile.

Two additional levels of grid refinement were employed near the rotor and in the wake region. An intermediate level of resolution of 0.75m was employed in a region $-0.73d \leq x \leq 1.77d$, $-0.94d \leq y \leq 0.94d$ and $-1d \leq z \leq 0.61d$ around the centre of the rotor, where x is the streamwise co-ordinate, y is the cross-stream co-ordinate, and z is the vertical coordinate. The rotor region was further refined with a homogeneous dimension of 0.1875 m in a region $-0.18d \leq x \leq 1.44d$, $-0.67d \leq y \leq 0.67d$, $-0.67d \leq z \leq 0.61d$. The final mesh contained approximately 2.8×10^6 elements.

The turbine blades are represented with the actuator line method (detailed below). The actuator lines are swept through the static mesh, thus no rotating sub-domains or mesh interfaces are required, as would be typical for blade-resolved models. This represents a significant saving in computational cost. It should however be noted, as described above, that the mesh is refined close to the turbine in order to resolve the large velocity gradients that occur around the blades.

C. Actuator line model

The turbine was represented using the actuator line method of Sørensen & Shen [26] implemented in OpenFOAM as a user-defined shared object library. The actuator line model represents the turbine blades with rotating lines along which force is applied to the flow, each line corresponding to one blade. The actuator forces therefore represent an additional term in the momentum equations. The in-house model has been extensively validated against a number of reference turbines, see for example Schluntz & Willden [27] and Wimshurst & Willden [28].

The blade forces are calculated using 2D blade element theory at 100 collocation points distributed cosinusoidally along the blade length in order to capture the changes in blade forces in the root and tip regions. The lift and drag data that were employed are described in Section III. The flow field around each blade was sampled using the potential flow equivalence method proposed by Schluntz & Willden [27], and reimposed on the flow using the Gaussian smearing technique of Sørensen & Shen [26]. The calculated blade forces were modified by the tip loss model of Shen et al. [29] to account for the 3D flow effects that reduce the blade forces near the tips.

The turbine nacelle, radius $R_{hub} = 1.35$ m, was represented using a cell-blocking method developed by Zormpa [30], following [31]. This method blocks fluxes into cells by applying a sufficiently large body force to the selected cells, thus enforcing the velocity to be zero. This method enables impermeable bodies to be represented in the numerical domain without requiring the geometry to be explicitly resolved.

Fig. 2 shows the converged ebb and flood flow profiles, noting in particular the reduction in near-surface flow speeds at higher speeds of the ebb tide. This was not present in the field data on the flood tide. The hub height turbulence intensity ranged between circa 8 – 20% for the highest to lowest flow speeds respectively.

V. Results

As shown in Fig. 3, the rotor is situated near the middle of the velocity profile and hence the freestream flow speed presented to the blades varies substantially each rotation. The flow speed appears to reduce at the top of the domain due to the surface shear stress during the ebb tide. As the turbine occupies a substantial portion of the water depth, acceleration of the flow was observed to be greater above and below the turbine than in the lateral directions.

A. Spanwise loading distribution

Fig. 4 shows the spanwise distribution of axial and tangential forces per unit span throughout the ebb and flood tides. Note that the rotational speed of the turbine Ω is fixed for all cases at 13.78 rpm, which means that the tip speed ratio $\lambda = R\Omega/U_\infty$, where U_∞ is the hub-height mean flow speed, varies between $\lambda = 18.55$ for $U_\infty = 0.7$ ms^{-1}, $\lambda = 4.64$ for $U_\infty = 2.8$ ms^{-1}, and $\lambda = 3.71$ for $U_\infty = 3.5$ ms^{-1}.

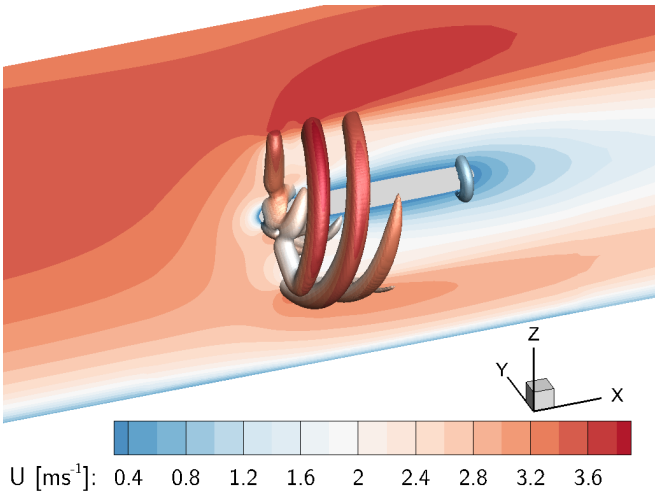

Fig. 3. Vertical profile at the centre of the domain of axial flow U past the turbine for the ebb tide, hub-height flow speed $U_\infty = 3.5\,\mathrm{ms}^{-1}$ case. Flow is from left to right. The nacelle region is blanked out in grey in the centre of the image. Q-criterion isosurface included to highlight the shed tip vortices.

Negative tangential forces per unit span (F_{tn}) are observed at radial positions $r/R < 0.35$ due to the blending of the turbine blade into a cylinder at $r/R = 0.228$, as discussed in Section III. Slight differences in the radial location where F_{tn} becomes positive occur due to the increase in angle of attack and therefore larger lift force and rotation of the resultant force towards the rotational direction as the flow speed increases. At the lowest flow speeds, given the blade twist distribution, the angle of attack along the blade is generally less than zero, resulting in small tangential and axial forces.

Fig. 4 also shows the how the spanwise force distribution varies throughout a rotation. The minimum and maximum force distributions are selected based on the forces per unit span at the $r/R = 0.90$ location, which corresponds approximately to the location where the forces per unit span are largest along the blade.

The minimum forces for both the flood and ebb tides occur when the blade is at $\theta = 160°$, where the blade angle $\theta = 0°$ corresponds to the blade being in the top-dead-centre position. There is a slight difference between the angular position of the blade when the maximum forces occur between the flood and ebb tides due to the different velocity profiles for the two cases. In the flood tide, the maximum F_{ax} occurs at $\theta = 336°$, compared to $\theta = 324°$ during the ebb tide. Maximum F_{tn} occurs at approximately $\theta = 346°$ for both tides.

The difference in angular position between maximum axial and tangential locations corresponds to a height difference of 0.46 m between the two locations. The magnitude of the tangential force is dominated by the difference in the lift and drag force contributions, which are both functions of the angle of attack, whereas the magnitude of the axial force is dominated the flow speed, hence the different angular positions at which the forces are maximum. Angular offset of the azimuthal location of minimum and maximum blade loads due to the velocity shear profile have also been observed by other investigators, for example [16] and [32].

The fluctuation range of the forces increases with flow speed. This is a function of the fixed rotational speed of the turbine. The tip speed of the rotor $R\Omega = 12.99\,\mathrm{ms}^{-1}$, which dominates the axial flow speed variations for the lower flow speed cases ($U_\infty = 0.7\ \mathrm{ms}^{-1}$ and $U_\infty = 1.4\ \mathrm{ms}^{-1}$). Consequently, the incident flow speed relative to the blade $V \approx \sqrt{U_\infty^2 + (r\Omega)^2}$ is almost constant throughout the rotation. The higher flow speed cases also see more significant flow speed fluctuations due to the shear profile, and hence larger variations in the spanwise forces are observed. If the rotational speed of the turbine is varied to maintain a constant tip speed ratio ($\lambda = 4.64$), then the magnitude of the velocity fluctuations relative to the rotational speed will be greater for lower flow speeds than for the $\Omega = 13.78$rpm case. Consequently, the load fluctuations experienced at the lower flow speeds will be greater in magnitude than in the fixed rotational speed case, albeit still smaller than those experienced at the higher flow speeds.

At a flow speed $U_\infty = 3.0\ \mathrm{ms}^{-1}$, in the ebb tide the axial force per unit span at $r/R = 0.90$ fluctuates about a mean of $\overline{F_{ax}}(r/R = 0.90) = 74.68\ \mathrm{kNm}^{-1}$ by $6.03\ \mathrm{kNm}^{-1}$. Due to the shear profile, this fluctuation is $+2.96\%/-5.11\%$ around the mean. A similar vertical asymmetry is noted for the tangential force per unit span, which fluctuates by $3.66\ \mathrm{kNm}^{-1}$ or $+9.74\%/-14.81\%$ around a mean value of $\overline{F_{tn}}(r/R = 0.90) = 14.93\mathrm{kNm}^{-1}$ in the ebb tide. The more uniform flow profile during the flood tide at $u = 3.0\ \mathrm{ms}^{-1}$ means that these fluctuations are larger in magnitude and more evenly distributed around the mean loads. For the ebb tide, the mean axial force per unit span $\overline{F_{ax}}(r/R = 0.90) = 72.19\ \mathrm{kNm}^{-1}$ fluctuates by $+5.29\%/-7.35\%$, or $9.13\ \mathrm{kNm}^{-1}$, and the tangential force per unit span fluctuates around a mean of $\overline{F_{tn}}(r/R = 0.90) = 13.58\mathrm{kNm}^{-1}$ by $+14.99\%/-18.21\%$, or $4.51\ \mathrm{kNm}^{-1}$.

B. Blade root loads

The variation of shear force and bending moment reacted at the root of the blade with respect to blade rotational position are given in Fig. 5 for ebb and flood flow speeds of $U_\infty = 3\ \mathrm{ms}^{-1}$. The shear force and bending moment in the axial direction are approximately 6 times larger than in the tangential direction. The flood shear profile in Fig. 2 presents a greater vertical variation than ebb flow, this is clearly reflected in the load variation acting on the blades with flood showing greater load variation from top dead center and bottom dead centre in Fig. 5. For similar reasons, the shear force and bending moment are always larger throughout the rotation for the turbine in the ebb tide than in the flood tide as the reduced shear across the rotor plane means that, on average, the flow speed incident on the blade, and therefore the loads at the blade root, are higher.

The variation in axial shear force and axial root bending moment throughout a rotation is dominated by the shear profile, whereas larger rotational asymmetry is observed in the tangential direction, in particular for

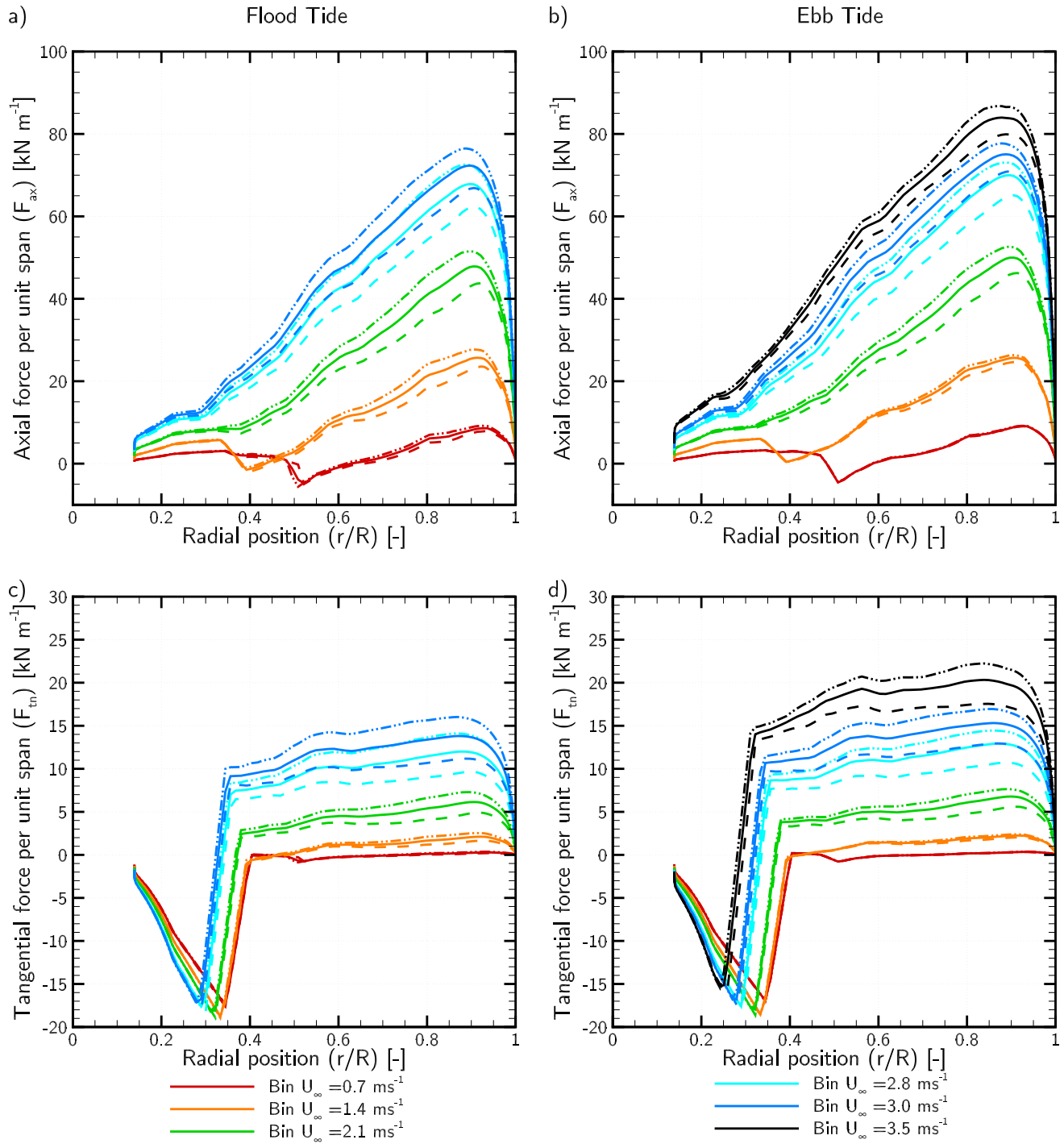

Fig. 4. Spanwise distribution of axial (a & b) and tangential forces (c & d) per unit span throughout the flood (a & c) and ebb (b & d) tides. Data are binned by mean hub-height velocity for the flood and ebb tides. Solid lines represent the mean, dashed lines the minimum and dot-dashed lines the maximum forces through a rotation.

the root bending moment. As discussed in Section V-A, the maximum tangential root bending moment does not occur at the top-dead-centre position, but rather as the blade is approaching this position. This effect is particularly emphasised in the flood tide with the tangential root bending moment varying by almost 33%, significantly more than in the ebb tide. Consequently, while the mean blade root loads are higher during the ebb tide, the fluctuations are more significant, and thus have the potential to be more damaging, during the flood tide.

VI. Conclusion

Differences in the vertical shear profile between flood and ebb tides can have a significant impact on the loads experienced by a turbine. These differences can be due to the different flow speeds reached during the tides, or due to differences in the flow that cause changes in the shape of the shear profile itself. Turbine blades experience in these flow speed variations as once-per-revolution fluctuations in blade loads, which leads to the accumulation of fatigue damage over the turbine lifetime.

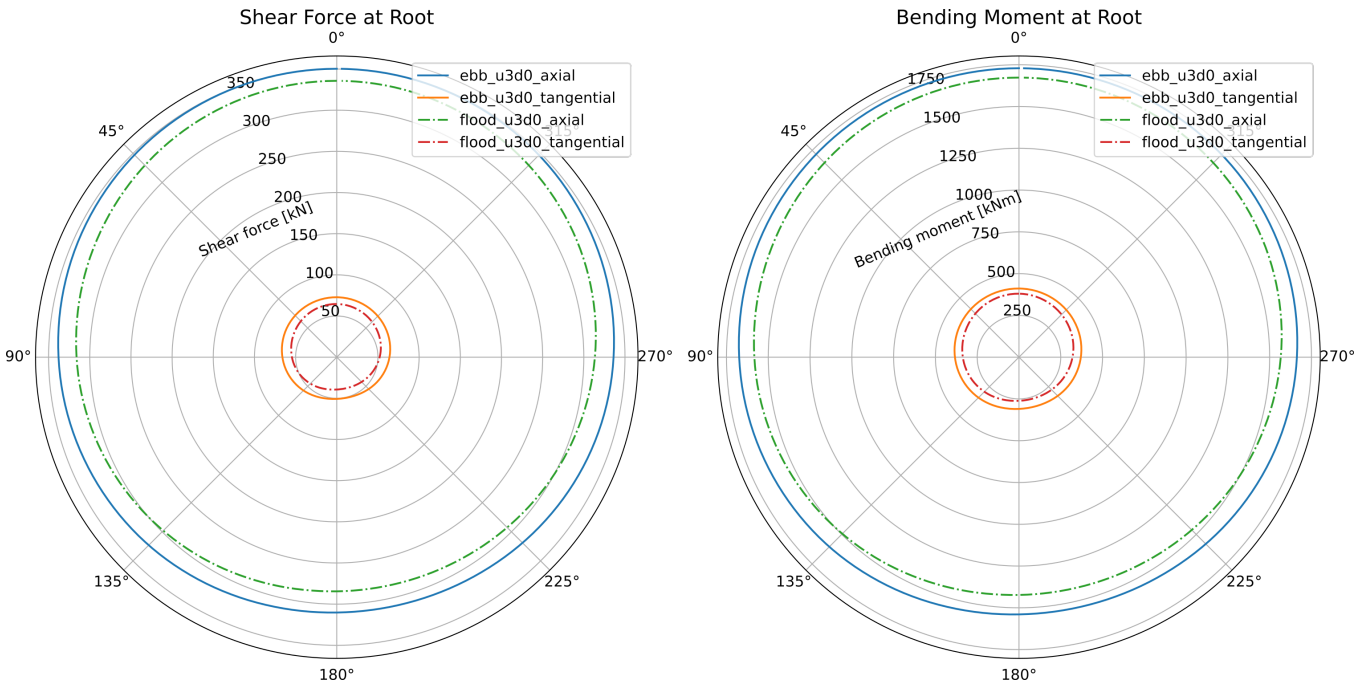

Fig. 5. Shear force (left) and bending moment (right) resolved in the axial and tangential directions at the blade root with respect to blade position. The hub-height flow speed $U_\infty = 3.0\,\mathrm{ms}^{-1}$ for both the flood (dot-dash lines) and ebb (solid lines) tides. $0\,\mathrm{deg}$ is taken as top dead centre.

Numerical methods that can capture the once-per-revolution sampling of flow speed variation by the blades are required. The actuator line turbine representation embedded within an unsteady RANS simulation has been shown to be capable of doing this, and avoids the additional computational expense involved in resolving blade geometry. The dissipative nature of RANS turbulence closures presents a challenge for the extension of this work to also considering the impact of discrete turbulent structures.

The mean forces, averaged over a rotation, acting on the blade were found to be higher during the ebb tide than the flood tide for all the hub-height velocities considered in this study. This is due to the reduced velocity shear across the rotor plane in the ebb tide at the Fall of Warness site. Blade loads fluctuations were found to be larger in the flood tide as the blades experienced greater variation in the oncoming flow speed throughout each rotation. Whilst the forces are larger in the axial direction, the relative variation in tangential forces was found to be greater. This is attributed to the changing angle of attack throughout each rotation.

The velocity profile was also found to have a significant impact on the blade root shear force and bending moment throughout the rotation. In the axial direction, the minimum and maximum loads occurred very close to the top and bottom-dead-centre positions whereas in the tangential direction a rotational offset was observed, similar to what has been reported in previous experimental and numerical studies. As with the spanwise loads, it was found that the axial and tangential shear force and bending moment were larger throughout the rotation for the ebb tide, but that the absolute and relative magnitude of variation was larger during the flood tide. Consequently, fatigue damage is expected to accumulate at different rates between the two tides.

This work is being extended to conduct accelerated fatigue testing on a decommissioned tidal turbine blade, with loading applied to the blade based on the simulated load distributions.

Acknowledgement

The authors would like to thank B. Sellar for providing flow data. C.R.V. and T.T. would like to thank M. Zormpa and X. Sheng for their help setting up simulations. C.R.V. and T.T. would like to acknowledge the use of the University of Oxford Advanced Research Computing (ARC) facility in carrying out this work. http://dx.doi.org/10.5281/zenodo.22558

References

[1] P. Liu and B. Veitch, "Design and optimization for strength and integrity of tidal turbine rotor blades," *Energy*, vol. 46, pp. 393–404, 2012.

[2] T. Adcock, S. Draper, R. Willden, and C. Vogel, "The fluid mechanics of tidal stream energy conversion," *Annual Review of Fluid Mechanics*, vol. 53, pp. 287–310, 2021.

[3] S. Muchala and R. H. J. Willden, "Influence of support structures on tidal turbine power output," *Journal of Fluids and Structures*, vol. 83, pp. 27–39, 2018.

[4] I. Milne, R. Sharma, R. Flay, and S. Bickerton, "The role of waves on tidal turbine unsteady blade loading," in 3^{rd} *International Conference on Ocean Energy*, ser. ICOE, Bilbao, Spain, 2010.

[5] T. Adcock, S. Draper, G. Houlsby, A. Borthwick, and S. Serhadlıoğlu, "Tidal stream power in the Pentland Firth - long-term variability, multiple constituents and capacity factor," *Proc. Institution of Mechanical Engineers, Part A*, vol. 228, pp. 854–861, 2014.

[6] B. Sellar and D. Sutherland, "Tidal energy site characterisation at the Fall of Warness, EMEC, UK," University of Edinburgh, Edinburgh, UK, Tech. Rep. MA1001, 2015.

[7] M. Lewis, S. Neill, P. Robins, M. Hashemi, and S. Ward, "Charateristics of the velocity profile at tidal-stream energy sites," *Renewable Energy*, vol. 114 Part A, pp. 258–272, 2017.

[8] M. Thiébot, J.-F.Filipot, C. Maisondieu, G. Damblans, C. Jochum, L. Kilcher, and S. Guillou, "Characterization of the vertical evolution of the three-dimensional turbulence for fatigue design of tidal turbines," *Philosophical Transactions of the Royal Society A*, vol. 378, p. 20190495, 2020.

[9] S. Evans, S. Dana, P. Clausen, and D. Wood, "A simple method for modelling fatigue spectra of small wind turbine blades," *Wind Energy*, vol. 24, pp. 549–557, 2021.

[10] P. Jeffcoate, R. Starzmann, B. Elsaesser, S. Scholl, and S. Bischoff, "Field measurements of a full scale tidal turbine," *International Journal of Marine Energy*, vol. 12, pp. 3–20, 2015.

[11] M. Allmark, R. Martinez, S. Ordonez-Sanchez, C. Lloyd, T. O'Doherty, G. Germain, B. Gaurier, and C. Johnstone, "A phenomenological study of lab-scale tidal turbine loading under combined irregular wave and shear flow conditions," *Journal of Marine Science and Engineering*, vol. 9, p. 593, 2021.

[12] J. McNaughton, B. Cao, C. Vogel, and R. Willden, "Model scale testing of multi-rotor arrays designed to exploit constructive interference effects," in 13^{th} *European Wave and Tidal Energy Conference*, ser. EWTEC, Naples, Italy, 2019.

[13] J. McNaughton, B. Cao, S. Ettema, F. Z. de Arcos, C. Vogel, and R. Willden, "Experimental testing of the performance and interference effects of a cross-stream array of tidal turbines," in 4^{th} *International Conference on Renewable Energies*, ser. RENEW, Lisbon, Portugal, 2020.

[14] G. Payne, T. Stallard, and R. Martinez, "Design and manufacture of a bed supported tidal turbine model for blade and shaft load measurement in turbulent flow and waves," *Renewable Energy*, vol. 107, pp. 312–326, 2017.

[15] J. McNaughton, R. Sinclair, and B. Sellar, "Measuring and modelling the power curve of a commercial-scale tidal turbine," in 11^{th} *European Wave and Tidal Energy Conference*, ser. EWTEC, Nantes, France, 2015.

[16] U. Ahmed, D. D. Apsley, I. Afgan, T. Stallard, and P. K. Stansby, "Fluctuating loads on a tidal turbine due to velocity shear and turbulence: Comparison of CFD with field data," *Renewable Energy*, vol. 112, pp. 235–246, 2017.

[17] S. Draycott, J. Steynor, A. Nambiar, B. Sellar, and V. Venugopal, "Experimental assessment of tidal turbine loading from irregular waves over a tidal cycle," *Journal of Ocean Engineering and Marine Energy*, vol. 5, pp. 173–187, 2019.

[18] R. M. Horwitz and A. E. Hay, "Turbulence dissipation rates from horizontal velocity profiles at mid-depth in fast tidal flows," *Renewable Energy*, vol. 114, pp. 283–296, 2017.

[19] M. K. McWilliam, T. K. Barlas, H. A. Madsen, and F. Zahle, "Aero-elastic wind turbine design with active flaps for AEP maximization," *Wind Energy Science*, vol. 3, pp. 231–241, 2018.

[20] F. Z. de Arcos, C. Vogel, and R. Willden, "Hydrodynamic modelling of flexible tidal turbine blades," in 13^{th} *European Wave and Tidal Energy Conference*, ser. EWTEC, Naples, Italy, 2019.

[21] B. Sellar, "Metocean data set from the redapt tidal project: Batch 1, part 2," 2017. [Online]. Available: https://doi.org/10.7488/ds/1687.

[22] B. Sellar, G. Wakelam, D. Sutherland, D. Ingram, and V. Vengatesan, "Characterisation of tidal flows at the european marine energy centre in the absence of ocean waves," *Energies*, vol. 11, no. 1, 2018. [Online]. Available: https://www.mdpi.com/1996-1073/11/1/176

[23] C. L. Ladson, C. W. B. Jr., A. S. Hill, and D. W. Sproles, "Computer program to obtain ordinates for NACA airfoils," NASA Langley Research Center, Hampton, Virginia, USA, Tech. Rep. 4741, 1996.

[24] D. Marten, J. Wendler, G. Pechlivanoglou, C. N. Nayeri, and C. O. Paschereit, "QBlade: An open source tool for design and simulation of horizontal and vertical axis wind turbines," *International Journal of Emerging Technology and Advanced Engineering*, vol. 3, pp. 264–269, 2013.

[25] F. Menter, M. Kuntz, and R. Langtry, *Ten years of industrial experience with the SST turbulence model*. Begell House, Inc., 2003.

[26] J. N. Sørensen and W. Z. Shen, "Numerical modelling of wind turbine wakes," *Journal of Fluids Engineering*, vol. 124, pp. 393–399, 2002.

[27] J. Schluntz and R. H. J. Willden, "An actuator line method with novel blade flow field coupling based on potential flow equivalence," *Wind Energy*, vol. 18, pp. 1486–1495, 2015.

[28] A. Wimshurst and R. H. J. Willden, "Analysis of a tip correction for horizontal axis turbines," *Wind Energy*, vol. 20, pp. 1515–1528, 2017.

[29] W. Z. Shen, J. N. Sørensen, and R. F. Mikkelsen, "Tip loss correction for actuator/Navier-Stokes computations," *Journal of Solar Energy Engineering*, vol. 127, pp. 209–213, 2005.

[30] M. Zormpa, "Towards multi-turbine CFD modelling using the actuator line method," University of Oxford, Oxford, UK, Tech. Rep., 2021.

[31] D. D. Apsley, T. Stallard, and P. K. Stansby, "Actuator-line CFD modelling of tidal-stream turbines in arrays," *Journal of Ocean Engineering and Marine Energy*, vol. 4, pp. 259–271, 2018.

[32] B. Gaurier, P. Druault, M. Ikhennicheu, and G. Germain, "Experimental analysis of the shear flow effect on tidal turbine blade root force from three-dimensional mean flow reconstruction," *Philosophical Transactions of the Royal Society A*, vol. 378, p. 20200001, 2020.